

Are basal Ediacaran (635 Ma) post-glacial “cap dolostones” diachronous?

Paul F. Hoffman^{a,*}, Galen P. Halverson^b, Eugene W. Domack^c, Jonathan M. Husson^a,
John A. Higgins^a, Daniel P. Schrag^a

^a *Department of Earth and Planetary Sciences, Harvard University, 20 Oxford St., Cambridge, MA 02138, USA*

^b *School of Earth and Environmental Sciences, The University of Adelaide, Adelaide, SA 5005, Australia*

^c *Department of Geology, Hamilton College, Clinton, NY 13323, USA*

Received 12 December 2006; received in revised form 16 March 2007; accepted 17 March 2007

Available online 27 March 2007

Editor: H. Elderfield

Abstract

A layer of shallow-water dolostone (“cap dolostone”) with idiosyncratic sedimentary structures was deposited across continental margins world-wide in the aftermath of the terminal Cryogenian snowball Earth. The dolostone has a global average thickness of 18.5 m and is interpreted stratigraphically in different ways in the current literature: as diachronous (top and bottom) and tracking glacioeustatic flooding, as semi-diachronous (bottom diachronous, top isochronous) and outlasting the flood, or as isochronous (top and bottom) and recording ocean-wide changes over time subsequent to deglaciation. Each interpretation carries a different implication for the timescale of cap dolostones and their isotopic signatures, and therefore for their origin.

In northern Namibia, we studied the Keilberg cap dolostone (635 Ma) across the Otavi carbonate bank and down a contiguous submarine paleoslope to estimated depths of ~0.5 km. We find giant wave ripples and other wave-generated structures in all areas, including the lower slope, pointing to a base-level change of large amplitude. No other formation in the carbonate succession contains wave-generated bedforms on the lower slope.

Carbon isotope records from the bank are similar in shape and absolute value, irrespective of thickness. Slope records are also similar to one another, but different in shape and value from those on the bank. If the cap is isochronous, lower-slope waters were enriched in ¹³C by 2–3‰ compared with the bank, which seems improbable. If diachronous, the lower slope, upper slope and bank records collectively describe a sigmoidal $\delta^{13}\text{C}$ curve over time with a net decline of 4.4‰. In addition, a lateral gradient of 1.0‰/100 km existed from the inner to outer bank.

If the flooding was rapid (<10 kyr), as suggested by ice-melting models, the $\delta^{13}\text{C}$ change may reflect strong surface warming, methane release, and kinetic isotope effects associated with rapid carbonate production. If the transgression was prolonged (>100 kyr), as implied by actualistic interpretation of paleomagnetic reversals in this and other cap dolostones, the $\delta^{13}\text{C}$ change could record Rayleigh distillation associated with the drawdown of a large atmospheric CO₂ reservoir, built up during the preceding snowball glaciation. Either way, the sedimentology and isotopes support the diachronous interpretation, and are inconsistent with the semi-diachronous and isochronous models. The base-level rise of ~0.5 km implies a glacioeustatic origin,

* Corresponding author. Tel.: +1 617 496 6380; fax: +1 617 384 8249.

E-mail address: hoffman@eps.harvard.edu (P.F. Hoffman).

meaning that cap dolostone sedimentation was synchronous with land ice melting. This leaves the actualistic interpretation of reversal frequency and speed in cap dolostones in conflict with ice-melting models.

© 2007 Elsevier B.V. All rights reserved.

Keywords: cap dolostone; cap carbonate; Ediacaran; Neoproterozoic; snowball Earth; carbon isotopes

1. Introduction

The last snowball Earth episode ended in 635 Ma [1] with the deposition of meters to decameters of dolomite ($[\text{CaMg}]\text{CO}_3$) on continental margins and inland seas world-wide (Table 1). “Cap dolostones” [2,3] represent a unique perturbation in the saturation state of the ocean. They sharply overlie terminal glacial strata (or an equivalent hiatus) and typically underlie limestones or fine-grained clastics of deeper water origin. The genesis of cap dolostones and their significance with respect to the glaciation continue to be debated [3–17], but many

agree that they accompanied a major marine transgression (rise in relative sea level), presumed to reflect the melting of continental ice sheets. In terms of sequence stratigraphy, cap dolostones form the transgressive systems tract of the post-glacial depositional sequence [9]. If the average ice thickness over all continents, continental shelves and banks (40% of global surface area) was 1.0 km [18–22], its melting would have caused a glacioeustatic rise of 0.6 km, equivalent to ~ 0.45 km after hydroisostatic adjustment (assuming densities of 3.3 and 2.9 g cm^{-3} for mantle and crust, respectively).

Table 1
Thickness of basal Ediacaran post-glacial cap dolostones [3] on different paleocontinents and margins

Paleocontinent	Location	Glacigenic unit	Cap dolostone	Thickness ^{a,b}	Reference
Amazonia	SW Brazil	Puga	Mirassol d'Oeste	24 m ^{*(?)} (1)	[45,16]
Arabia	NE Oman	Fiq	Hadash	4.5 m (8)	[68]
Arctic Alaska	NE Brooks Range	none	Nularvik	35 m (8)	[69]
Australia	Central Australia	Olympic	Mount Doreen	4 m (2)	[3]
	South Australia	Elatina	Nuccaleena	5 m (6)	[70] Paul F. Hoffman, unpubl. data
	Tasmania	Cottons Breccia	Cumberland Creek	6 m (2)	[71]
	Western Australia	Landrigan	Lower Ranford	8.5 m (2)	[3]
Baltica	Finnmark	Smalfjord	Lower Nyborg	5 m (4)	[72]
Congo	NW Namibia	Ghaub	Keilberg	38 m (49)	This work
	Shaba–Zambia	Petit Conglomérat	Calcaire Rose	10 m (1)	[73]
	West Congo	Upper Tilliod	C1	10 m	[74]
India	Lesser Himalaya	Blaini	Upper Blaini	>5 m (5)	[65,75]
Kalahari	SW Namibia	Numees	Bloeddrif	24 m (10)	Francis A. Macdonald, unpubl. data; Paul F. Hoffman, unpubl. data
	W Namibia	Blässkranz	Toms	21 m (3)	Paul F. Hoffman, unpubl. data
Laurentia	NW Canada	Stelfox (Icebrook)	Ravensthorpe	12 m (20)	[7] Paul F. Hoffman, unpubl. data
	California	Surprise	Noonday	175 m* (5)	[76]
	East Greenland	Storeelv	Lower Canyon	10 m (6)	[77] Paul F. Hoffman, unpubl. data
	East Svalbard	Wilsonbreen	Lower Dracöisen	10 m (8)	[78]
	Scotland–Ireland	Stralinchy–Reelan	Cranford	4 m (3)	[79]
South China	South China	Nantuo	Lower Doushantuo	4 m ^{*(?)} (14)	[12] Paul F. Hoffman, unpubl. data
Tarim	Quruqtagh, NW China	Tereeken	Lower Zhamoketi	6.3 m (3)	[41]
West Africa	Algeria	Fersiga	Oued Djouf	<6 m*	[5]
	Mauritania	Jbéliat	Amogjar	5 m* (15)	[80] Paul F. Hoffman, unpubl. data
	Burkina–Fasso	Lower Sud-Banboli	Middle Sud-Banboli	1.5 m* (3)	[14].

^a Average thickness of cap dolostone *sensu stricto* (number of measured sections in brackets).

^b Asterisk indicates cap dolostone is top-truncated by a subaerial exposure surface.

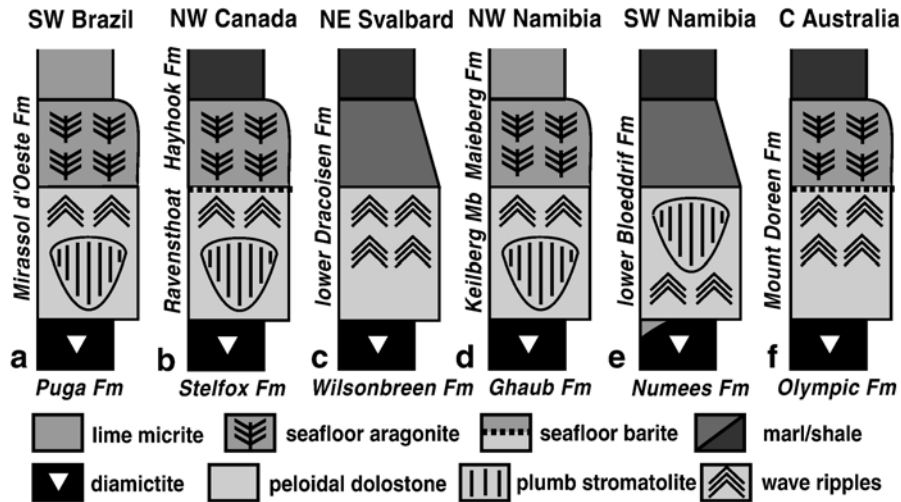


Fig. 1. Sequence of lithofacies and sedimentary structures in basal Ediacaran post-glacial cap dolostones and related limestones on different paleomargins (Table 1).

Cap dolostones and related limestones (“cap carbonates” sensu lato) display a panoply of unusual sedimentary features, which occur in a broadly consistent vertical sequence on different paleomargins (Fig. 1). The sequence has been interpreted in three basically different ways. If the cap dolostone is isochronous (Fig. 2a), meaning that its base and top are approximately the same age everywhere, the vertical sequence must represent basin-wide environmental changes over time. For example, deposition of cap dolostone has been

attributed to time-dependent gas-hydrate destabilization and methane oxidation [12]. If isochronous, the cap dolostone must have been deposited in different water depths. If its deposition followed glacioeustatic flooding [12], the timescale would not be limited by the estimated ice-sheet meltdown time of $\sim 2\text{--}10$ kyr [21]. A second possibility is that the cap dolostone is semi-diachronous (Fig. 2b), meaning that its base is diachronous and tracked the glacioeustatic transgression, but its top is isochronous. For example, the switch in sedimentation

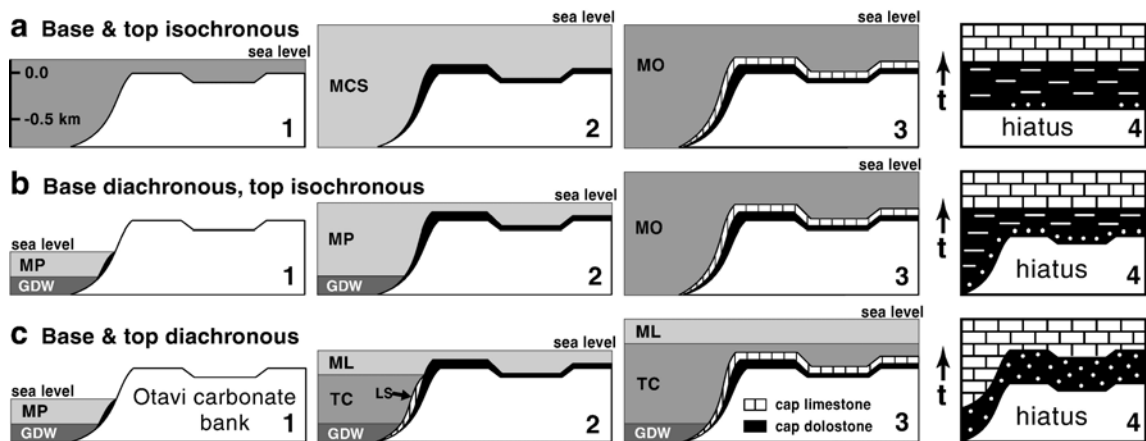


Fig. 2. Time-dependent models for post-glacial cap dolostone and limestone deposition. (a) Isochronous model: 1, depth–distance section during glacioeustatic rise, no carbonate deposited; 2, cap dolostone deposited, according to [8,11,12] in response to methane cold seepage (MCS); 3, cap limestone deposited in response to change in ocean chemistry (MO, mixed ocean); 4, time–distance section of cap dolostone (black, dots show shallower water, dashes deeper water) and cap limestone (bricks). (b) Semi-diachronous model: 1, cap dolostone deposited from incipient meltwater plume (MP) above glacial deep water (GDW); 2, meltwater plume grows and floods the bank, cap dolostone deposited diachronously; 3, limestone deposited, according to [15] in response to mixing of MP and GDW; 4, time–distance section. (c) Diachronous model: 1, same as b1; 2, meltwater plume differentiates a mixed layer (ML), which deposits cap dolostone, and a thermocline (TC), which simultaneously deposits limestone (LS); 3, TC floods the bank, causing diachronous change from dolostone to limestone at the ML–TC interface, an oxic–anoxic boundary in the meltwater column [17]; 4, time–distance section.

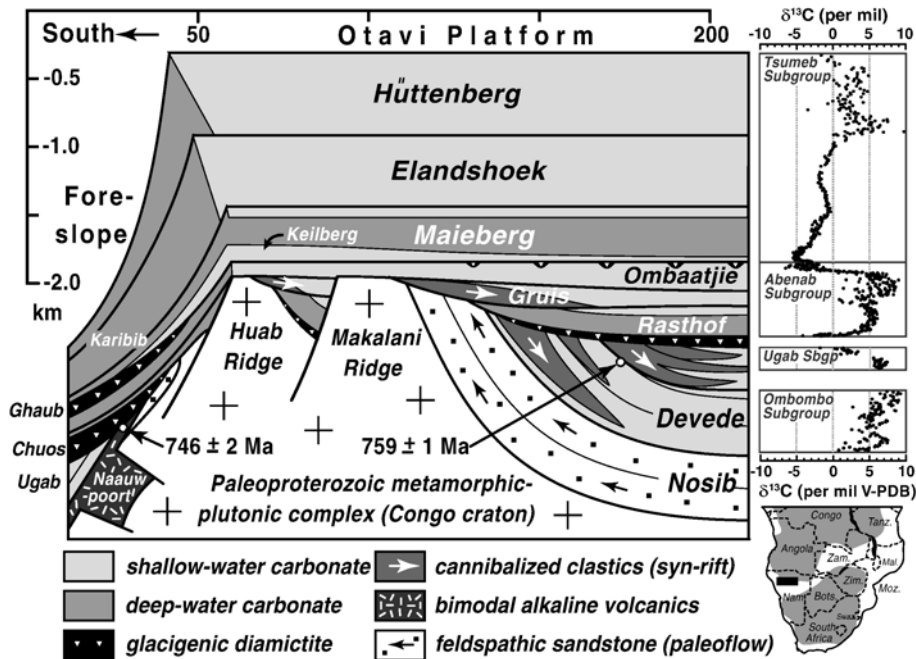


Fig. 3. North–south stratigraphic cross-section and composite carbon isotope record of the Otavi Group on the southern and western flanks of the Kamanjab inlier (Fig. 2a), Namibia [24]. Inset map of southern Africa gives location of Fig. 2a (black rectangle) relative to the Congo and Kalahari cratons (shaded).

from cap dolostone to overlying limestone has been attributed to ocean-wide mixing of saline glacial deep water and a low-density meltwater plume [15]. If the stable density stratification outlasted the glacioeustatic flood [15], the timescale for cap dolostone sedimentation would once again not be limited by the meltdown time. A third option is that cap dolostones are wholly diachronous (Fig. 2c), with bottoms and tops that are older or younger according to paleoelevation. If cap dolostone sedimentation tracked the glacioeustatic flood, it could have been deposited in the same range of water depths everywhere. Environmental changes over time would be reflected by differences between sections from lower and higher areas. A basin-wide event might register at the top of the dolostone in low areas and at the bottom in high areas. The timescale for deposition of any given section would be only a fraction of the overall cap dolostone timescale, which itself must be less than the meltdown time, assuming that dolostone sedimentation began when some grounded ice had already melted. The timescale over which the deposition occurred is critical to any interpretation of cap dolostones and their isotopic characteristics as this will determine the relative importance of ocean mixing, warming, gas exchange, and carbonate or silicate weathering.

In this study, we employ field sedimentology and $\delta^{13}\text{C}_{\text{carb}}$ isotopic measurements from paleogeographi-

cally well-characterized sections of the 635-Ma Keilberg (pronounced *kile'-baireg*) cap dolostone in northern Namibia [23,24], to determine if it is diachronous, semi-diachronous or isochronous. The diachronous transition from cap dolostone to limestone [17] will be treated in detail in a forthcoming paper incorporating data from Namibia and Canada.

2. Paleogeography and development of the Otavi carbonate bank

Between ~ 770 Ma [24] and ~ 580 Ma [25,26], the (present) southwestern promontory of the Congo craton was a slowly-subsiding marine bank (platform), maintained by the deposition of ~ 3 km of dominantly shallow-water carbonate strata of the Otavi Group (Fig. 3). The strata are exposed in an arcuate fold belt that rims the craton in northern Namibia. The southern edge of the bank is intersected in a structurally simple homocline on the south flank of Kamanjab Inlier (Fig. 4). To the south lies a distally-tapered wedge of slope- and basin-facies carbonates (debris flows and rhythmites). The western two-thirds of the Fransfontein homocline (Fig. 4b) run east–west, approximately parallel to inferred paleoslope contours; the eastern third angles northeastward (up the paleoslope) to the bank-edge on farm Danubé 59 near Gros Tutara [27]. Subaerial exposure surfaces and

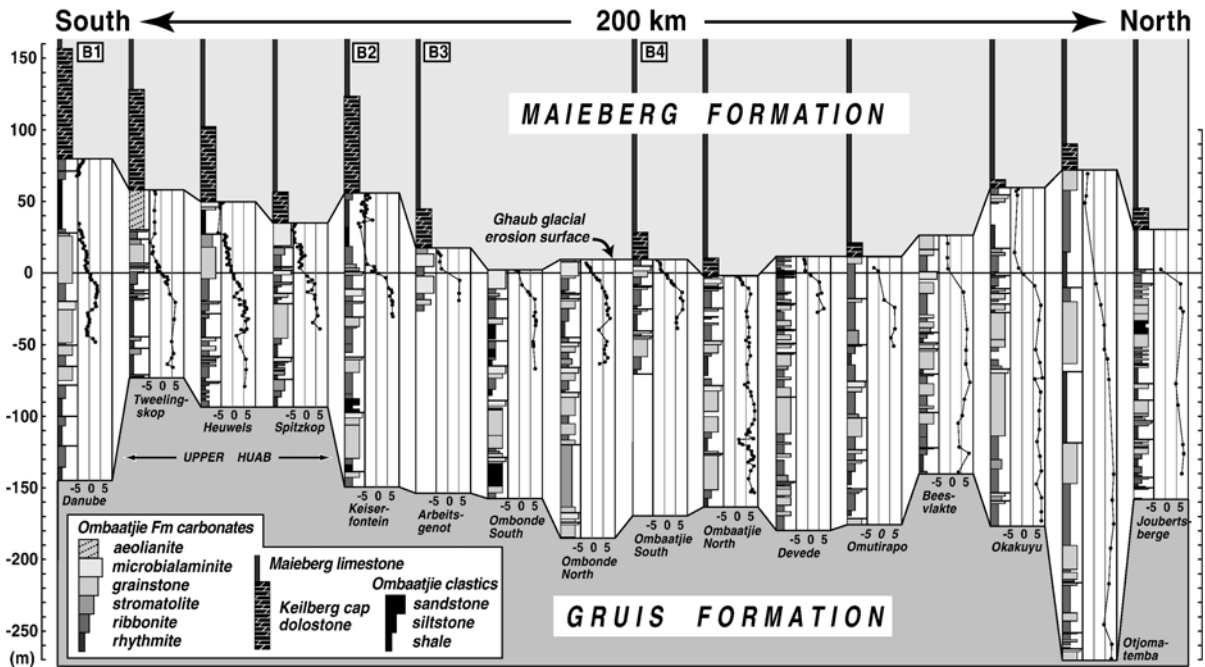


Fig. 5. Variation in thickness of the Keilberg cap dolostone across the Otavi carbonate bank, relative to post-glacial topography inferred from stratigraphic height above a datum based on the 0‰ crossing of the pre-glacial Trezona $\delta^{13}\text{C}$ anomaly [28]. Note thickening of cap dolostone on the raised outer (southern) rim of the bank.

containing zircons dated by U–Pb ID-TIMS at 635.5 ± 0.5 Ma [23,1]. The cap dolostone (Keilberg Member) above the Ghaub Formation (or its equivalent hiatus) has been correlated with the basal Ediacaran cap dolostone at the GSSP in South Australia [32,23,33,24]. An isochronous decline of more than 10‰ in $\delta^{13}\text{C}_{\text{carb}}$ (Fig. 3) occurred in the last 1.0 Myr before the glacioeustatic fall [28]. This isotopic datum provides a measure of differential erosion across the bank resulting from base-level fall and the subsequent glaciation (Fig. 5). It also demonstrates that no significant structural rotation occurred on the bank at the time of the Ghaub glaciation (contra [34]).

A preliminary account of foreslope stratigraphy on the Fransfontein homocline (Fig. 4b) is given in [27,35]; see also Fig. S1 in Appendix A). The foreslope is divided into stratigraphically-distinct upper and lower slopes (Fig. 6). The boundary between them is located roughly 5 km seaward of the bank-edge (Fig. 4b). Assuming a topographic gradient similar to the western slope of the present Great Bahama Bank [36,37], the upper–lower slope boundary would correspond to a paleodepth of ~0.5 km below the bank-edge. The lower slope, 5–10 km south of the projected bank-edge, would represent paleodepths of 0.5–0.7 km. These are conservative estimates because the western slope of the Great Ba-

hama Bank is a mud-dominated, leeward margin with a maximum slope inclination of 8.0° (excluding the scarp at the top of the slope, believed to result from Quaternary glacioeustatic fluctuations). This is 2–3 times less steep than typical windward carbonate slopes [37]. Stratigraphic relations between the Otavi bank and slope are tricky, but three levels can be confidently correlated based on lithology and carbon isotopes: the Rasthof Formation

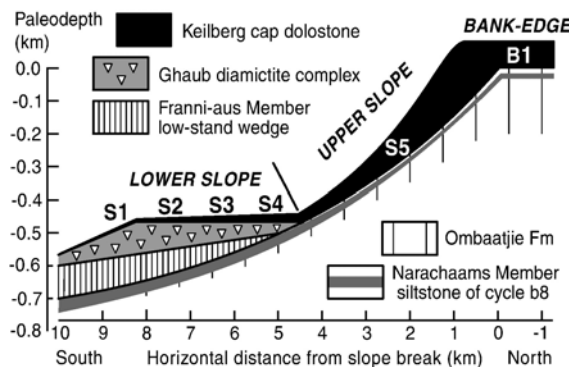


Fig. 6. Schematic stratigraphic relations on the lower and upper foreslope of the Otavi carbonate bank [27], as exposed on the Fransfontein homocline (Fig. 4b).

(cap carbonate of the Chuos glaciation), the Narachaams (*nar'-a-khams*) Member (terrigenous siltstone marker in the Ombaatjie Formation cycle b8 on the bank that thickens downslope), and the combined Keilberg cap dolostone and overlying Maieberg (*my'-baireg*) limestone ([27,35]; Fig. S1 in Appendix A).

A major base-level fall, presumably caused by ice-sheet growth at higher latitudes, preceded the glaciation of the bank. The top of the bank was exposed, carbonate aeolianite accumulated at the bank-edge, and an upward-coarsening wedge of carbonate turbidites and debris flows (Franni-aus Member) accumulated on the lower foreslope [27]. The more proximal debris flows are rich in partially-disaggregated clasts of well-sorted, very coarse-grained oolite. The oolite is sedimentologically diagnostic of strongly-agitated waters but no source for it is known on the bank. Isotopically, the low-stand wedge is depleted ($\delta^{13}\text{C}$ of 0 to -4% , Fig. S1 in Appendix A), similar to the last marine carbonate deposited on the bank before the fall (upper part of Ombaatjie cycle b8, Fig. S1 in Appendix A). The oolite is inferred to have originated on the foreslope as the strandline fell. Stranded oolite was subject to gravitational mass wasting, resulting in debris flows and turbidites as observed.

Glaciation of the bank itself caused erosion of the bank and upper foreslope, and deposition of glacially-transported debris on the lower foreslope. A complex of polymictic, grounding-zone diamictites is intertongued with thinner intervals of well-stratified proglacial detritus, variably-rich in ice-rafted debris [38,27]. The diamictites include ice-contact, proximal “rain-out”, and resedimented deposits [39]. They are heterolithic and variably derived from the low-stand wedge and the upper Ombaatjie Formation on the bank (Fig. 5). Sedimentologically, the Ghaub Formation resembles Quaternary ice grounding-zone wedges on sub-polar marine shelves (e.g., [40]), except for its composition (all carbonate debris) and paleobathymetry. Instead of being on the bank or upper slope, like Quaternary wedges, the Ghaub wedge is situated on the lower slope, ~ 0.5 km below the bank-edge according to our estimated slope profile (Fig. 6). This implies a large base-level fall, thick subtropical ice, or a combination of the two. A detailed sedimentological analysis of the Ghaub wedge on the lower slope is in preparation.

In the central part of the Fransfontein homocline (Fig. 4b), a glacial-age trough cuts out the low-stand wedge (Fig. S1 in Appendix A). A double-crested moraine of massive diamictite, 600 m high by 7.5 km wide at the base, stands in the middle of the trough. The trough and moraine are ascribed to a paleo-ice stream [27].

Away from the moraine, the grounding-zone wedge is terminally draped by a decimeter of well-stratified debris flows and contourites, choked with stone- and boulder-size IRD. This unit is distinctly reddish-brownish in color, suggesting Fe and Mn enrichment. The Keilberg cap dolostone overlies it conformably with a transition consistently less than 0.5 cm thick. This abrupt transition signals an essentially simultaneous cessation of IRD delivery (tiny stones are rarely found a few cms into the dolostone), a drape of clay-size marl, and onset of peloidal dolomite production. The cessation of IRD is taken to indicate when the upstream ice line retreated landward from the strand.

The Ghaub Formation is absent from the upper foreslope and outer (more southerly) bank, but reappears discontinuously, invariably at the same horizon, on the inner (more northerly) bank (Fig. 3). The bank-top glacial deposits consist of sheared and unsheared diamictites, possibly lodgement tills, that are typically less than 2 m thick. Wherever present, the diamictite is overlain directly by Keilberg cap dolostone, which elsewhere rests disconformably on strata of the upper Ombaatjie Formation (Fig. 5).

4. Sedimentology of the Keilberg cap dolostone on the bank and slope

The Keilberg cap dolostone [31] is a laterally continuous layer of very pale grey, tannish or pinkish tinted, erosion-resistant dolomite. It is 65–75 m thick on the outer bank and tapers to 15–20 m on the inner bank. The taper is not due to differential accommodation. On the contrary, it is thicker on the elevated rim of the bank and thinner in the more-eroded interior (Fig. 5). On the slope, the cap dolostone tapers from 65–105 m on the upper slope to 5–10 m on the lower slope. Its overall area-weighted average thickness is ~ 38 m, an order of magnitude greater than examples in East Gondwana (Table 1) often misrepresented as archetypical.

A smooth, knife-sharp disconformity separates the cap dolostone from the underlying Ombaatjie Formation or Franni-aus Member. The contact with the Ghaub Formation is conformable (see above) but lithologically abrupt (<0.5 cm). There is virtually no evidence of significant hiatus, reworking, or subaerial exposure. The upper contact of the cap dolostone is everywhere conformable and lithologically gradational across 1–2 m of strata into marly limestone rhythmite.

Sedimentologically, the cap dolostone can be divided into five lithofacies, which have specific stratigraphic and paleogeographic distributions (Fig. 7). The most widespread lithofacies is mechanically-laminated on an

mm-scale, with characteristic medium- to mostly small-scale, low-angle, cross-stratification (Fig. 8a,b). The primary sediment clearly consisted of coarse silt- to coarse sand-size particles. Locally, primary peloidal grains <3 mm in diameter are clearly visible (Fig. 8b), similar to those described in correlative cap dolostones on other paleocontinents [3,7,12,16,41,78]. The peloids form graded and reverse-graded laminae, typically draped by a veneer of micropeloids. The coarsest peloids (Fig. 8b) occur in strongly-winnowed sections on the steep flanks of the Duurwater moraine [27]. The lamination type and abundant low-angle cross-stratification indicate deposition above normal wave base in a dynamic wave-dominated regime. This conclusion applies to all the sections studied, including those on the lower slope (Fig. 7).

A variant of the laminated peloidal dolostone lithofacies is distinguished by the presence of “giant

wave ripples” [42]. The ripples are trochoidal in section, with sharp crests and broadly curved troughs, and the crestlines are linear and parallel (Fig. 8c,d). Their synoptic relief is typically ~0.3 m and crestal spacing ~1.5 m. Coherent ripple sets aggrade over 1.0–2.5 m vertically. Their azimuthal crestal orientations are $150 \pm 35^\circ$ on both the bank and slope, strongly oblique to the bank-edge, the inferred slope contours and tectonic strike (Fig. 4). These extraordinary bedforms are interpreted to have formed under the influence of perpetual (not hurricane or tsunami) waves with unusually-long wave periods [42]. Sustained windspeeds exceeding 20 m s^{-1} over infinite fetch, or $\sim 3 \times$ normal trade windspeeds, are hindcasted from gravity wave theory. Giant wave ripples occur preferentially in the upper part of the cap dolostone on both the inner bank and lower slope (Fig. 7). They do not occur in the stromatolitic facies that dominates the outer bank and upper slope. Excellent examples (Fig. 8c,

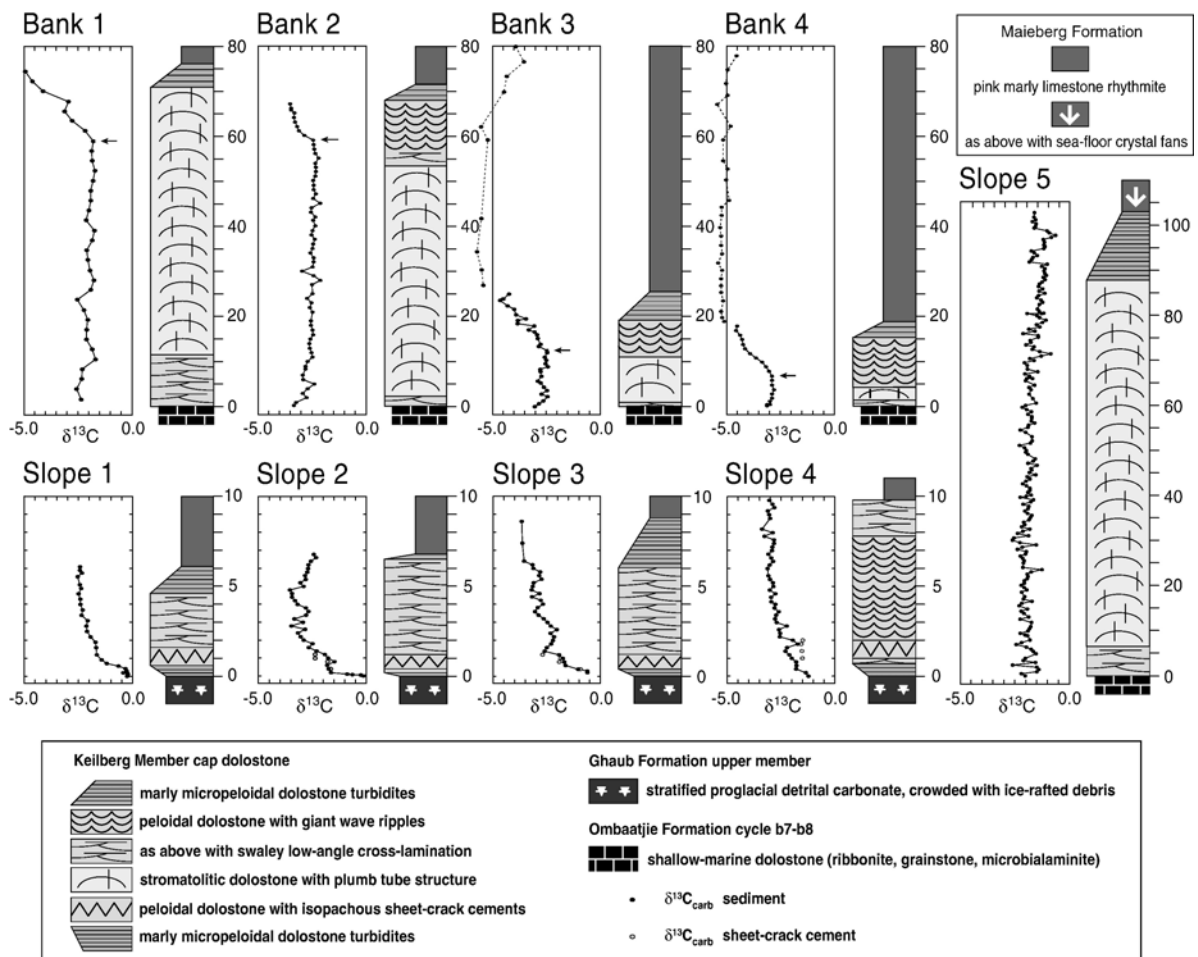


Fig. 7. Lithofacies logs and carbon isotope records for sections of the Keilberg cap dolostone on the Otavi bank (B1 to B4), lower foreslope (S1 to S4), and upper foreslope (S5). Note difference in scale between the lower slope sections and those on the upper slope and bank.

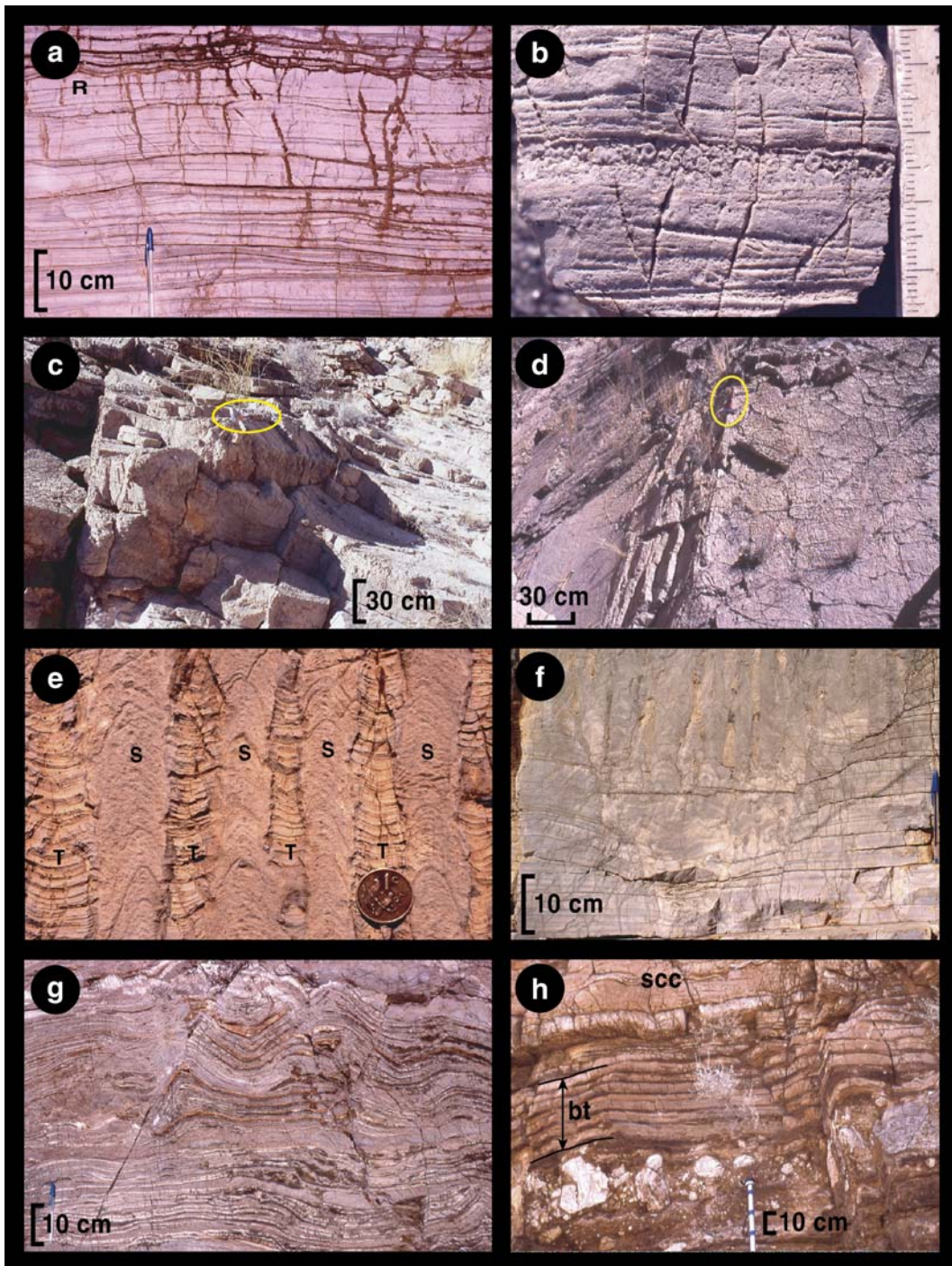


Fig. 8. Characteristic lithofacies of the Keilberg cap dolostone. Coin (2 cm), pen (15 cm) and hammer (33 cm) for scale. Peloidal dolostone (a) with low-angle cross-stratification and small-scale wave ripples (R), near base of section B4. Macro-peloids (b) on the east flank of the Duurwater moraine [27] on the lower foreslope. Giant wave ripples [42], in oblique section (c) and plan (d), on the lower foreslope at S 20° 12.072', E 15° 04.278', between sections S2 and S3. Internal structure of plumb stromatolite (e) from inner bank section B4, showing walls of stromatolite (S) with arched microbial lamination and "tubes" (T) of abiotically laminated micrite. Origination point of plumb stromatolite (f) within mechanically-laminated peloidal dolostone near the base of bank section B4. Isopachous sheet-crack cements (g) in peloidal dolostone near the base of lower-slope section S1. Basal turbidites (bt) and sheet-crack cement (scc) overlying IRD (Ghaub Formation) in lower-slope section S1 (h).

d) of giant wave ripples occur at many locations on the lower slope between sections S3 and S4 (Fig. 4b). If these sections represent paleodepths of >0.5 km below the slope break, and if the ripples formed in water depths of less than 0.4 km at most [42], then the bank must have been emergent while the cap dolostone was being deposited in the lower slope.

Stromatolites (considered here to be laminated buildups of microbially-bound sediment) form large-scale (1–10 m), confluent, domical-laminated masses that dominate the outer bank and upper slope sections (Fig. 7). They are subtly laminated and consist of heavily-recrystallized, micropeloidal(?) dolostone lacking millimetric peloids. The domical laminae have broad arches and steep flanks. Discontinuous m-scale tubes, typically 2 cm in diameter, are contained exclusively within stromatolites (Fig. 8e,f), never in the mechanically-laminated facies. They are invariably oriented in the paleo-vertical, or plumb, irrespective of the attitude of the host lamination. The tubes are filled by multiple generations of void-filling cements and by remnants of primary, non-microbial dolomicrite, laminated normal to the tube axes. The stromatolites and plumb tubes are strikingly similar to those in the correlative cap dolostones of Death Valley, California [43,44] and Mato Grosso, Brazil [45,16]. The stromatolites are much less recrystallized on the inner shelf, where the tubes are closely-spaced and filled by laminated dolomicrite alone, no void-filling cement (Fig. 8e). The stromatolites form a continuous layer of conjoined, beet-shaped masses, 2–3 m in diameter, flanked by mechanically-laminated sediment devoid of tubes (Fig. 8f). The tubes originated as sediment-filled, stably-located, pit-like depressions on actively-aggrading, microbially-bound, stromatolite surfaces. Locally, the tubes morph into vertical sheets, forming small-scale “gutters” in plan view, oriented subparallel to the giant wave-ripple crests. We agree with the interpretation [44] that the tube structure is a product of microbial-sediment interaction under extreme environmental forcing, perhaps high accumulation rate, but we are not satisfied that the plumb orientation of the tubes has been adequately explained. The tubes invariably appear above the base of the cap dolostone (Fig. 8f), and there is no structural or isotopic evidence that they formed by methane escape from glacial-age permafrost or submarine gas hydrate [8]. It seems reasonable to assume that the stromatolites accreted under the influence of cyanobacteria in the photic zone. Their ability to trap and bind particulate sediment [46] accounts for the positive correlation between stromatolite development and local thickness of cap dolostone (Fig. 7).

The lower 0.5–1.0 m of mechanically-laminated dolostone on the lower slope (Fig. 7) undulates on a meter-scale due to differential vertical jacking of sheet-crack complexes (Fig. 8g). The cracks are filled by fibrous, isopachous dolomite (\pm late quartz) cement. The cracks and their fills apparently formed close to the sediment–water interface, and imply that the pore-fluid was overpressured, critically oversaturated, and subject to an alkalinity pump. The cements have $\delta^{13}\text{C}$ values consistently within 0.5‰ of the host sediment (Fig. 7). The zone of sheet-cracks is laterally continuous at outcrop and map scales, varying in density, but does not form centered complexes like methane cold seeps.

A few decimeters of sediment density flows or turbidites (Fig. 8h) occur at the base (below the sheet-crack zone) of most lower-slope sections (Fig. 7). The flow units are relatively continuous, normally-graded, and 1–2 cm thick. They are composed of dolomicrite grading upward to marlstone, rarely the reverse. Evidence of wave action is lacking. Assuming they were deposited below wave base, the change upward into low-angle cross-stratified peloidal strata represents an initial regression that goes against the overall transgressive sequence. This initial regression is tentatively attributed to local base-level fall caused by the instantaneous loss of gravitational attraction to the Otavi ice sheet as it melted away [47].

The upper part of the cap dolostone in all areas consists of thin-bedded, dolomicrite–marlstone couplets (sediment density flows), with only very low-aspect undulose bedforms. They represent water depths beyond the reach of long-period waves responsible for giant wave ripples. At their top, they grade smoothly over 1–2 m vertically into recessive rhythmite composed of alternating bands of pinkish limestone, marlstone and allodapic (gravitationally resedimented) dolostone. The rhythmite was deposited below wave base, undulose layers superficially resembling “ribbon” facies are the result of tectonic shear in the rheologically weak limestone. The rhythmite includes the maximum flooding stage of the cap-carbonate depositional sequence [9]. It marks the nadir in $\delta^{13}\text{C}_{\text{carb}}$ of -5.5‰ in both the bank and lower-slope sections [24]. Crystal fans of pseudomorphosed aragonite form localized masses of sea-floor cement, up to 100 m thick, in the lower rhythmite on the upper slope (Fig. 7), the outer bank [48] and the Duurwater moraine [27]. The carbonate content and thickness of rhythmite decrease down the slope [17]. On the bank, the rhythmite grades upward into a 0.3-km-thick highstand tract bounded by a well-developed subaerial exposure surface. The same sequence boundary can be roughly located isotopically on the slope [24],

where the entire cap-carbonate sequence is $\sim 6\times$ thinner than on the bank (65 vs 400 m).

5. Carbon isotopes

Stable carbon isotope ratios were measured by methods previously described [24] in micro-drilled powders of closely-spaced samples from four sections on the bank, one on the upper slope, and four on the lower slope (Fig. 7). Bank section B1 is at the bank-edge, B4 is ~ 100 km from the bank-edge, and B2 and B3 are at an intermediate distance (Fig. 4a). B2 overlies a basement structural high, Makalani Ridge (Fig. 3), and is nearly $3\times$ thicker than B3, ~ 300 km to the east, which is not known to overlie a basement structure. For ease of

comparison, color-coded composite $\delta^{13}\text{C}$ and $\delta^{18}\text{O}$ records from the bank and slope are shown in Fig. 9. The bank records are standardized to a common thickness, and adjusted for time-varying differences in sedimentation rate (see below). The $\delta^{18}\text{O}$ records are shown despite their greater susceptibility to alteration by migrating porewaters. The data do contain more scatter than for $\delta^{13}\text{C}$, although we cautiously interpret the $\delta^{18}\text{O}$ data as representing a relatively closed system due to presumed low permeability of the dolomite, with some diagenetic overprint (e.g., section B2). Consistent spatial and temporal patterns exist in both data sets.

The $\delta^{13}\text{C}$ records from the bank are broadly similar (yet subtly different), both in form and absolute value, despite their four-fold range in stratigraphic thickness

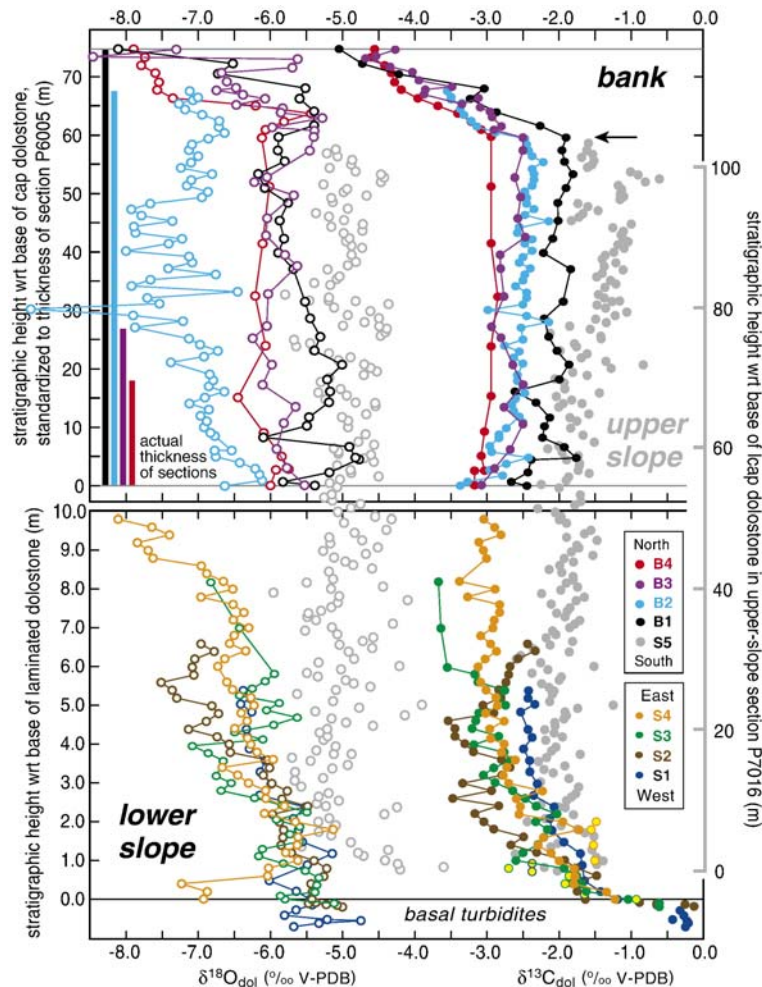


Fig. 9. Color-coded composite $\delta^{13}\text{C}$ and $\delta^{18}\text{O}$ records (see Fig. 4 for locations) for the Keilberg cap dolostone on the Otavi bank (above) and slope (below). Note different scales of lower slope, upper slope and bank records. Bank records are standardized to the inflection point (arrow) and total thickness of bank-edge section B1. Actual thickness of bank sections shown by color bars. Note north–south isotope gradient in bank records, and overall sigmoidal trajectory of slope and bank records combined.

(shown by vertical color bars in Fig. 9). They begin near -3.0‰ PDB (-2.5‰ at the bank-edge) and end at roughly -4.5‰ . Section B2 ends $\sim 1.0\text{‰}$ heavier because the top of the section was not sampled (Fig. 7) due to surficial weathering. Each record consists of two segments, joined at an inflection (indicated by arrows in Fig. 7). The first segment rises slowly by $\sim 0.5\text{‰}$ and the second falls rapidly by $1.5\text{--}3.0\text{‰}$. The inflection does not correspond to any lithologic change: it occurs in continuous stromatolites at B1 and in the giant wave-rippled interval elsewhere. The second segment coincides with sharply-rising concentrations of Mn and Fe, especially acid-soluble Fe, an $\sim 5\text{‰}$ rise and subsequent $\sim 10\text{‰}$ fall in $\delta^{34}\text{S}_{\text{CAS}}$, and a fall in $\delta^{18}\text{O}_{\text{carb}}$ [17]. The large difference in total thickness between the outer (B1–2) and inner (B3–4) bank sections (Fig. 7) is mainly a function of the first segment of the isotope curve: the second segments differ only by a factor of 1.45 (16 m, B1; 12 m, B2; 13 m, B3, and 11 m, B4). Accordingly, the records are standardized in the composite plot to a common inflection point (arrow in Fig. 9).

The first (slowly-rising) segments of the bank records are systematically offset (Fig. 9) from north to south. The bank-edge record (B1) persists $\sim 1.0\text{‰}$ heavier than the most distant record (B4), ~ 100 km to the north. Intermediate values persist in the two sections ~ 50 km north of the bank-edge (B2 and B3), despite their 300-km separation parallel to the bank-edge (Fig. 4a) and their almost three-fold difference in total thickness (Fig. 7). The upper-slope record (S5) persists $\sim 0.5\text{‰}$ heavier than the bank-edge section (B1).

The lower-slope records also decline in $\delta^{13}\text{C}$ up-section, but are different in form and value from those on the bank. They are concave-upward and begin at substantially higher values than any bank sample (Fig. 9). All values greater than -1.0‰ are from the basal centimetric density flows (Figs. 7 and 8h). As they are not present in all sections, we use the base of the low-angle cross-laminated lithofacies as the datum (Fig. 9). The tails of the slope records project onto the first segment of the bank records. The late steep decline in $\delta^{13}\text{C}$ observed in all bank records is nowhere found on the slope (Fig. 7), indicating that the top of the cap dolostone is older on the slope than on the bank. Taken together, the lower slope and bank records define a sigmoidal path beginning around -0.2‰ and ending around -4.6‰ .

The lower slope records come from a stretch of the Fransfontein homocline that roughly parallels the inferred paleoslope contours (Fig. 4b). This is reflected in the isotope records, which have broadly similar trajectories and range of values (Fig. 9). However, the

most easterly section (S4) is $\sim 30\%$ thicker than the others, has no basal density flows, begins at a lower $\delta^{13}\text{C}$ value (-1.23‰), has well-developed giant wave ripples and a prolonged isotopic tail. It is a reasonable supposition that S4 was situated higher on the lower slope than the other sections (Fig. 7).

The (103-m-thick) upper-slope record is isotopically the heaviest of any section (Fig. 9). It rises slowly by $\sim 1.0\text{‰}$ overall, similar to the first segments of the bank records and the tails of the lower-slope records (Fig. 7). Missing are the early steep decline of the lower-slope records and the late steep decline of the bank records. This fits the prediction of the diachronous model for an intermediate section (Fig. 2c). The exact placement and scaling of the upper-slope isotopic record in Fig. 9 is therefore arbitrary, but reflects our inference that it bridges the gap (in time) between the tail of the lower-slope records and the slow early rise of the bank records.

6. Discussion

6.1. Sedimentary structures

Sedimentary structures (giant wave ripples, low-angle cross-stratification, reverse-graded peloids) indicate that the bulk of the cap dolostone on the lower slope originated above wave base, the same as on the bank. Given that the estimated paleo-relief of at least 0.5 km exceeds the depth of wave base at the most extreme [42], the top of the bank must have been above sea level when the dolostone was accumulating on the lower slope. A diachronous cap dolostone and a large base-level rise are unavoidable if the paleo-relief estimate is valid. In its support, we note that the cap dolostone is the only unit in the entire Otavi Group hosting wave-generated bedforms on the lower foreslope.

The vertical asymmetry of the cap dolostone, tube stromatolites toward the base and giant wave ripples toward the top, is consistent with transgression (i.e., water depth increasing with stratigraphic height). Stromatolites formed in the shallow part of the mixed layer because of the limit of the photic zone in sediment-clouded waters. Giant wave ripples formed in the deep part of the mixed layer, where only long-period waves felt the bottom and interference from short-period waves was therefore absent [42]. The lack of wave-generated structures in the sediment density flows at the top of the cap dolostone suggests additional deepening stratigraphically above the giant wave ripples. The only deviation from the overall transgression is the presence of deeper water turbidites at the base of the lower-slope sections (Fig. 7 and 8h), which we attribute to non-

eustatic sea-level fall due to the loss of self-gravitation [47] of the disappearing ice sheet on the Otavi bank.

The magnitude of the transgression was such that the lower slope was above wave base at the outset, but the top of the bank was below wave base at the maximum flood (lower Maieberg Formation). It must have exceeded the paleo-relief of the Otavi foreslope. Only glacioeustasy could account for a base-level rise of 0.5 km, and then only if the average thickness of ice on all continents was over 1.0 km. Our explanation of the basal regression in lower-slope sections is temporally compatible with glacioeustatic flooding. If the Otavi ice sheet was located at low elevations in the subtropics, it would have disappeared before ice sheets melted at higher elevations and paleolatitudes. Subsequent glacioisostatic adjustment was accommodated within the highstand tract (upper Maieberg Formation, Fig. 3) of the depositional sequence.

6.2. Timescale

What was the timescale of deglaciation and glacioeustatic rise? We assume that floating ice (“sea glaciers”) disappeared before grounded ice sheets: it was thinner and its surface lower. Only grounded ice melting contributes to glacioeustasy. Ice-sheet melting models [49,21] and Quaternary analogues [50] suggest rapid deglaciation in 2–10 kyr driven by ice-albedo and ice-elevation feedbacks. This timescale is consistent with the occurrence of subaerial exposure surfaces at the top of cap dolostones in certain regions ([5,7,9], Fig. 11; [45]), assuming they resulted from glacioisostatic adjustment (timescale of 10^4 yr). The area-weighted average thickness of the Keilberg cap dolostone is ~ 38 m (Table 1), which implies a sedimentation rate of 3.8 – 19.0 mm yr $^{-1}$, averaged over the entire period of glacioeustatic rise. In the diachronous and semi-diachronous models (Fig. 2b,c), these must be minimum rates because any given section contains only a fraction of the total duration of cap-dolostone sedimentation. They are phenomenally high sedimentation rates for marine carbonate on a regional scale, but are qualitatively compatible with unique sedimentary structures in cap dolostones, including tube stromatolites [44] and giant wave ripples that aggrade up to 2.5 m of sediment in a single set [42].

In contrast, paleomagnetic evidence for geomagnetic polarity reversals and/or excursions within correlative cap dolostones in Brazil [51], Oman [52] and South Australia [53] imply a timescale 1–2 orders of magnitude longer than those derived from ice-melting models. Natural remanent magnetization in cap dolostones is stably carried by detrital hematite [54] and the primary paleopole in South Australia is known from

independent field tests [55,56]. High-resolution data, replicated in multiple parallel sections in South Australia [53], indicate that each reversal and/or excursion occupies a decimeter of section or less. The reversal frequency in 635 Ma is unknown, but the minimum timescale for a geomagnetic reversal of the present field is thought to be set by the electrical diffusion time of the solid inner core, or possibly its tangent cylinder: 3–5 kyr based on estimates of core conductivity [57]. This is consistent with a duration of 7 kyr for the Matuyama–Brunhes reversal (0.78 Ma) inferred from rapidly-deposited (>10 cm kyr $^{-1}$) North Atlantic drift sediments [58]. Similar sediment records indicate that geomagnetic excursions (which are $\sim 10\times$ more frequent than reversals) can occur in less than 2 kyr [59], supporting the hypothesis that excursions represent reversals of the liquid outer core which are not taken up by the solid inner core [57]. If we assume that the maximum thickness of 10 cm for a full reversal in the South Australian cap dolostone [53] represents ~ 5 kyr, then the total thickness of the cap of 5.0 m represents ~ 250 kyr, assuming a uniform sedimentation rate, ~ 0.02 mm yr $^{-1}$. This rate is slow for a relatively pure shallow-water carbonate. While terrigenous mud layers do occur in poorly-developed (<10.0 m thick) cap dolostones (Table 1), they constitute less than 10% of those sections and their accumulation rates averaged over 250 kyr [53] would not have exceeded ~ 0.002 mm yr $^{-1}$. This is 50–500 times slower than typical accumulation rates of post-glacial wind-blown dust (loess) of 0.1 – 1.0 mm yr $^{-1}$ [60,61]. It begs the question why cap dolostones, if deposited so slowly, were not swamped by terrigenous input under conditions of glacial retreat in predominantly terrigenous Cryogenian successions (e.g., Australia, NW Canada, NW China, East Greenland, Norway, Oman, East Svalbard).

We find it difficult to reconcile the paleomagnetically estimated sedimentation rate with the sedimentology of cap dolostones. An alternative, non-actualistic interpretation of the magnetostratigraphy is that reversal frequency and speed were 1–2 orders of magnitude greater than for the 0–300-Ma field. This implies a substantially weaker geomagnetic field intensity in 635 Ma, but paleomagnetic intensity data are lacking to test this conjecture. If the actualistic interpretation [51,53] is correct, then either the snowball meltdown was much slower than suggested by climate models, or the deposition of cap dolostones greatly exceeded the period of glacioeustatic rise (i.e., the semi-diachronous model). We test (and reject) the second option in the next section. We also discuss the quite different interpretations of the isotopic data implied by each timescale.

6.3. Isotopic records

The carbon isotopic records from the bank are mutually consistent, as are those from the lower slope (Figs. 7 and 9). They begin with similar values, end with similar values and describe similar trajectories, concave-down on the bank and concave-up on the lower slope. The bottoms and tops of the lower slope sections are on average 2.5 and 1.5‰ heavier, respectively, than the same parts of the bank sections. This is compatible with the diachronous model, and incompatible with both the isochronous and semi-diachronous models (Fig. 2).

The consistency of the $\delta^{13}\text{C}$ records from like settings (Fig. 9) indicates that they reflect secular changes in the isotopic and chemical composition of the ocean mixed layer (where the dolostone was deposited), and in its temperature. It is not supportive of secondary “organogenic” dolomitization [8,11,12,16], which leads to post-depositional scattering of $\delta^{13}\text{C}$ values [62].

What is the significance of the four-fold difference in thickness between the inner- and outer-bank sections (Fig. 7)? The difference is well-correlated with variation in the first (slowly-rising $\delta^{13}\text{C}$) segment of the records, which is ~60 m thick (80% of the total) on the outer bank but only ~7 m thick (38% of the total) on the inner shelf. It is weakly correlated with the second (rapidly-falling $\delta^{13}\text{C}$) segment of the records, which is only 5 m thicker on the outer bank compared with the inner bank. A simple explanation for the observed thickness variation is a higher sedimentation rate on the outer bank during the slowly-rising segment. Higher sedimentation rates on the outer bank cannot be explained by differences in accommodation. Erosion of the bank during emergence and glaciation left the bank with a raised outer rim (Fig. 5). The positive topography is correlated with the persistence of stromatolites, which dominate the thickest sections (Fig. 7). Initial topographic advantage may have allowed the stromatolites to maintain themselves in the photic zone as the bank was flooded. Sedimentation rate is the time-averaged rate of deposition minus erosion. The presence of microbial mats has a positive effect on sedimentation rate because it stabilizes fine granular sediment thereby lowering the erosion rate [46].

There are small but distinct differences in the range of $\delta^{13}\text{C}$ values in both bank and lower-slope records (Fig. 9). Differences in lower-slope records are subject to multiple interpretations because they are situated at somewhat different depths on the slope. The relative flatness of the bank top, less than 80 m of paleo-relief (Fig. 5), means that the cap dolostone there should be broadly synchronous, although the outer-bank records would, in the diachronous and semi-diachronous models, be slightly

younger at their base because of post-glacial topography on the bank (Fig. 5). This is consistent with higher basal $\delta^{13}\text{C}$ values at the bank-edge (B1), but not with the relatively low basal values at B2 (Fig. 7).

What is the significance of the persistent north–south isotopic gradient of ~1.4‰ between the inner bank and the upper slope during the slowly-rising $\delta^{13}\text{C}$ stage (Fig. 9)? During the melting of a snowball Earth, the surface ocean would be isotopically equilibrated to the large atmospheric CO_2 reservoir. Meltwater injection and surface warming would tend to suppress whole-ocean mixing [15]. Nevertheless, a temperature gradient might have existed between cold upwelling waters at the top of the slope and warm ponded waters in the interior of the bank. Higgins and Schrag [10] calculated that a temperature rise of 15 °C would cause $\delta^{13}\text{C}_{\text{carb}}$ to fall by 1.7‰, mainly due to reduced equilibrium fractionation between atmospheric CO_2 and calcite (or dolomite). Oxygen isotope records (Fig. 9) are in qualitative agreement with this interpretation: $\delta^{18}\text{O}_{\text{carb}}$ values decline systematically from south to north, highest on the upper slope and lowest in the bank interior (ignoring section B2, which appears to have exchanged with meteoric waters or at deep-burial temperatures). A salinity gradient, fresher off-bank and saltier on-bank, would have contributed to the observed $\delta^{13}\text{C}$ gradient, but it is not reflected in the $\delta^{18}\text{O}$ data (Fig. 9). An additional factor could be a kinetic isotope effect associated with CO_2 air–sea exchange, which results from the fact that isotopic equilibration occurs more slowly than the equilibration of CO_2 concentration [63]. At the upper slope and bank-edge, surface waters would be relatively cold if upwelling existed, but the upwelled water would warm up upon reaching the surface, resulting in CO_2 evasion and a slight increase in $\delta^{13}\text{C}$ comparable to that seen in modern upwelling areas [63]. However, this effect may be diminished if CO_2 concentrations were very high (snowball Earth hypothesis), as the isotopic equilibration rate would be enhanced (relative to the rate of CO_2 equilibration) due to the shift in carbon speciation at low pH towards dissolved CO_2 . Additional kinetic effects associated with spatial variation in saturation state are possible, but it is difficult to explain why there should be a systematic gradient from north to south.

A more fundamental aspect of the $\delta^{13}\text{C}$ records is the contrast between the lower slope, upper slope and bank (Fig. 9). Lower-slope records begin with steep declines from maximum values, bank records end with steep declines to minimum values, and the upper-slope record has no steep decline. This is consistent only with the diachronous model, in which the cap dolostone was deposited first on the lower slope, then on the upper

slope, and last on the bank. By implication, limestone rhythmite was accumulating below wave base on the lower slope while peloidal dolostone was being deposited above wave base on the bank (Fig. 2c). The transition from dolostone to limestone is not isochronous, but instead represents the migrating interface between surface waters that produced peloidal dolostone, and thermocline waters depositing limestone rhythmite and aragonitic sea-floor cements. At the maximum flooding stage, limestone rhythmite was accumulating in all areas and its $\delta^{13}\text{C}$ is correspondingly uniform at -5.5‰ ([24], Fig. 10). Thus, the isotopic data reinforce the inference from sedimentology, that when giant wave ripples and other wave-generated structures were forming on the lower slope, the bank-top, >400 m above, must have stood above sea-level. When those same structures were forming on the bank, the lower slope must have been well below wave base.

What caused the $\delta^{13}\text{C}$ of cap dolostone to fall by $\sim 4.4\text{‰}$ (from -0.2‰ to -4.6‰) on the timescale of post-glacial flooding? Higgins and Schrag [10] calculated that a 1.7‰ change (i.e., bank sections alone) could be accounted for by a 15 °C rise in temperature, or alternatively as a kinetic isotope effect associated with rapid carbonate production. Reverse ice-albedo feedback would drive a rapid temperature rise, given that the ocean would have a small heat capacity because of a stable density stratification due to meltwater production and surface warming. The $\delta^{18}\text{O}$ data (Fig. 9) are at least qualitatively compatible with rising temperature and falling salinity. Raising the temperature of the surface ocean by 30 °C would change $\delta^{13}\text{C}_{\text{carb}}$ by -3.4‰ [10]. This is still $\sim 1\text{‰}$ short of the observed change (Fig. 9). Rising salinity would have lowered $\delta^{13}\text{C}_{\text{carb}}$ in low-pH waters, but no complementary rise in $\delta^{18}\text{O}$ is observed. Glacioeustatic flooding would rapidly destabilize shallow methane hydrate (permafrost), causing the release of isotopically depleted carbon [64,8,11,65], but there is no convincing structural or isotopic evidence for methane cold seeps in the Keilberg Member. Kasemann et al. [66] inferred a massive transfer of CO_2 from the atmosphere to the ocean from boron isotopes in the Keilberg cap dolostone, which indicate a large drop in pH of surface waters during sedimentation. A kinetic isotope effect of this transfer would be a transient lowering of $\delta^{13}\text{C}_{\text{DIC}}$ [63]. This presents a third potential contributor to the secular decline in $\delta^{13}\text{C}$, providing we assume the more rapid ($<10\text{ kyr}$) timescale. The ability of the surface ocean to take up CO_2 would have depended on its ingredients: (1) meltwater from marine ice, which contains virtually no CO_2 ; (2) meltwater from meteoric ice (compressed snow), which has CO_2 concentrations

(as air bubbles or clathrate) ~ 0.1 that of cold seawater under equivalent atmospheric $p\text{CO}_2$ [67]; and (3) snowball deep water, which would have been CO_2 -laden from submarine volcanism and equilibration with the atmosphere by air–sea gas exchange through cracks in the ice, which would be efficient on the multimillion-year timescale of a snowball glaciation. If a massive transfer of CO_2 into the ocean did occur [66], a large flux of alkalinity or other means of CO_2 consumption (e.g., organic fixation and burial) must have operated in order to maintain carbonate saturation and deposit the cap dolostone. The kinetic isotope effect of CO_2 uptake would have been short-lived [63] and could only have contributed to the early steep decline in $\delta^{13}\text{C}$ of the lower-slope records (Fig. 9), assuming CO_2 concentrations were low enough for this mechanism to be viable.

Why is the cap dolostone distally tapered on the slope (Fig. 7)? In the isochronous model (Fig. 2a), this is easily explained through the effect of water depth on carbonate saturation. In the diachronous model, cap dolostone thickness depends on the accumulation rate and its duration, which is a function of the rate of base-level rise and the mixed layer depth. If the rate of ice-sheet melting diminished as the ice lines retreated poleward, rapid early rates of glacioeustatic rise would cause cap dolostones on the lower slope to be relatively thin. In addition, sections corresponding to depths within the mixed layer at the maximum lowstand must inevitably be truncated, to zero thickness at the lowest level ever touched by the mixed layer.

If the timescale for cap dolostones was not 2–10 kyr, as implied by climate models, but 100s of kyr, as inferred from magnetostratigraphy, then the -4.4‰ change in $\delta^{13}\text{C}_{\text{carb}}$ could be easily explained. Hoffman et al. [6] attributed part of this change to Rayleigh distillation associated with rapid drawdown of atmospheric CO_2 due to silicate weathering in the snowball aftermath. Kennedy et al. [8] countered that silicate weathering is too slow to lower $[\text{CO}_2]$ on the timescale of cap dolostone deposition, assuming rapid deglaciation. In response, Higgins and Schrag [10] proposed that carbonate weathering supplied the alkalinity flux driving cap dolostone sedimentation, and attributed the decline in $\delta^{13}\text{C}_{\text{carb}}$ to a kinetic isotope effect or temperature rise. If cap dolostones were deposited on a timescale of 100s of kyr, then the Rayleigh distillation hypothesis [6] would be plausible after all. We do not favor this interpretation, however, because it is difficult to reconcile with the world-wide distribution of cap dolostones and their sedimentology. It is inconsistent with evidence for isostatic “rebound” [5,7,9,45] because isostatic equilibrium would be maintained on a

timescale of 100s of kyr. This point should not be oversold, however, because the evidence for “rebound” is not convincing in all areas. Whichever timescale is correct, the overwhelming evidence that the Keilberg cap dolostone is diachronous and was associated with an extreme base-level rise means that its deposition cannot be separated in time from ice-sheet melting.

7. Conclusions

The existence of giant wave ripples and low-angle cross-stratification at an estimated paleodepth of 0.5 km below the carbonate bank-edge provides sedimentological evidence that the post-glacial Keilberg cap dolostone is diachronous, and was associated with a major marine flooding of glacioeustatic origin.

Carbon isotope records from the lower slope, upper slope and bank strongly support a diachronous interpretation and are incompatible with the semi-diachronous and isochronous models for this cap dolostone. The overall sigmoidal trajectory of $\delta^{13}\text{C}_{\text{carb}}$ over time, with a net fall of $\sim 4.4\%$, is incompletely sampled in any single section.

If the timescale for ice-sheet decay (and by implication cap dolostone sedimentation) was 2–10 kyr, as suggested by climate modeling, swiftly rising temperatures, gas-hydrate destabilization, and kinetic isotope effects associated with rapid carbonate production and gas transfer may together explain the secular change in $\delta^{13}\text{C}_{\text{carb}}$. If, on the other hand, the timescale was ~ 250 kyr, as implied by magnetostratigraphic records from cap dolostones, including the Keilberg, the change in $\delta^{13}\text{C}_{\text{carb}}$ could reflect Rayleigh distillation of a large atmospheric CO_2 reservoir, built up during a prolonged snowball Earth. Regardless of timescale, the evidence for diachroneity and a base-level rise of over 0.5 km means that deposition of the Keilberg cap dolostone occurred simultaneously with the melting of grounded ice sheets globally.

Acknowledgements

This study was funded by the U.S. National Science Foundation grant EAR-0417422 (Geobiology and Environmental Geochemistry Program), Harvard University and Hamilton College. We are grateful to the Geological Survey of Namibia, Edila Köhler of farm Danubé 59, and other farm owners and residents for the privilege of doing field work in Namibia. Enthusiastic field assistance was provided by Mary Beth Day, Woody Fischer, Tim Fox, John Higgins, Matt Hurtgen, Gabe Jostrom, Francis Macdonald, Corey Rennell, and James Saenz. Karla Knudsen, Winston Macdonald and Sarah Fawcett cheerfully prepared samples for isotopic

analysis, carried out by Greg Eiseheid in the Geochemical Oceanography Laboratory at Harvard. We acknowledge helpful discussions with Philip Allen, David Evans, Ian Fairchild, Woody Fischer, Michael Hambrey, Charlie Hoffmann, Jian Hong, Matt Hurtgen, Peter Huybers, Ganqing Jiang, Lee Kump, Francis Macdonald, Adam Maloof, Bernhard Peucker-Ehrenbrink, Susannah Porter, Tim Raub, Andy Ridgwell, Jeff Severinghaus, Graham Shields, Ricardo Trindade, and Shuhai Xiao. We thank Woody Fischer, Peter Huybers, Francis Macdonald and Tim Raub for their helpful comments on the draft manuscript, and peer-reviews by Graham Shields and Anne Nédélec which greatly improved the final product.

Appendix A. Supplementary data

Supplementary data associated with this article can be found, in the online version, at [doi:10.1016/j.espl.2007.03.032](https://doi.org/10.1016/j.espl.2007.03.032).

References

- [1] D. Condon, M. Zhu, S.A. Bowring, W. Wang, A. Yang, Y. Jin, U–Pb ages from the Neoproterozoic Doushantuo Formation, China, *Science* 308 (2005) 95–98.
- [2] G.E. Williams, Sedimentology, stable-isotope geochemistry and palaeoenvironment of dolostones capping late Precambrian glacial sequences in Australia, *J. Geol. Soc. Aust.* 26 (1979) 377–386.
- [3] M.J. Kennedy, Stratigraphy, sedimentology, and isotopic geochemistry of Australian Neoproterozoic postglacial cap dolostones: deglaciation, $\delta^{13}\text{C}$ excursions, and carbonate precipitation, *J. Sediment. Res.* 66 (1996) 1050–1064.
- [4] J.P. Grotzinger, A.H. Knoll, Anomalous carbonate precipitates: is the Precambrian the key to the Permian? *Palaios* 10 (1995) 578–596.
- [5] J. Bertrand-Sarfati, R. Flicoteaux, A. Moussine-Pouchkine, A. Ait Kaci Ahmed, Lower Cambrian apatitic stromatolites and phospharenites related to the glacio-eustatic cratonic rebound (Sahara, Algeria), *J. Sediment. Res.* 67 (1997) 957–974.
- [6] P.F. Hoffman, A.J. Kaufman, G.P. Halverson, D.P. Schrag, A Neoproterozoic snowball Earth, *Science* 281 (1998) 1342–1346.
- [7] N.P. James, G.M. Narbonne, T.K. Kyser, Late Neoproterozoic cap carbonates: Mackenzie Mountains, northwestern Canada: precipitation and global glacial meltdown, *Can. J. Earth Sci.* 38 (2001) 1229–1262.
- [8] M.J. Kennedy, N. Christie-Blick, L.E. Sohl, Are Proterozoic cap carbonates and isotopic excursions a record of gas hydrate destabilization following Earth’s coldest intervals? *Geology* 29 (2001) 443–446.
- [9] P.F. Hoffman, D.P. Schrag, The snowball Earth hypothesis: testing the limits of global change, *Terra Nova* 14 (2002) 129–155.
- [10] J.A. Higgins, D.P. Schrag, Aftermath of a snowball Earth, *Geophys. Geochem. Geosyst.* 4 (2003), [doi:10.1029/2002GC000403](https://doi.org/10.1029/2002GC000403).
- [11] G. Jiang, M.J. Kennedy, N. Christie-Blick, Stable isotopic evidence for methane seeps in Neoproterozoic postglacial cap carbonates, *Nature* 426 (2003) 822–826.

- [12] G. Jiang, M.J. Kennedy, N. Christie-Blick, H. Wu, S. Zhang, Stratigraphy, sedimentary structures, and textures of the late Neoproterozoic Doushantuo cap carbonate in South China, *J. Sediment. Res.* 76 (2006) 978–995.
- [13] A.J. Ridgwell, M.J. Kennedy, K. Caldeira, Carbonate deposition, climate stability, and Neoproterozoic ice ages, *Science* 302 (2003) 859–862.
- [14] S.M. Porter, A.H. Knoll, P. Affaton, Chemostratigraphy of Neoproterozoic cap carbonates from the Volta Basin, West Africa, *Precambrian Res.* 130 (2004) 99–112.
- [15] G.A. Shields, Neoproterozoic cap carbonates: a critical appraisal of existing models and the plume world hypothesis, *Terra Nova* 17 (2005) 299–310.
- [16] E. Font, A. Nédélec, R.I.F. Trindade, M. Macouin, A. Charrière, Chemostratigraphy of the Neoproterozoic Mirassol d'Oeste cap dolostones (Mato Grosso, Brazil): an alternative model for Marinoan cap dolostone formation, *Earth Planet. Sci. Lett.* 250 (2006) 89–103.
- [17] M.T. Hurtgen, G.P. Halverson, M.A. Arthur, P.F. Hoffman, Sulfur cycling in the aftermath of a 635-Ma snowball glaciation: evidence for a syn-glacial sulfidic deep ocean, *Earth Planet. Sci. Lett.* 245 (2006) 551–570.
- [18] W.B. Harland, Evidence of late Precambrian glaciation and its significance, in: A.E.M. Nairn (Ed.), *Problems in Palaeoclimatology*, Interscience, London, 1964, pp. 119–149.
- [19] D.A.D. Evans, Stratigraphic, geochronological, and paleomagnetic constraints upon the Neoproterozoic climatic paradox, *Am. J. Sci.* 300 (2000) 347–433.
- [20] Y. Donnadieu, F. Fluteau, G. Ramstein, C. Ritz, J. Besse, Is there a conflict between the Neoproterozoic glacial deposits and the snowball Earth interpretation: an improved understanding with numerical modeling, *Earth Planet. Sci. Lett.* 208 (2003) 101–112.
- [21] W.R. Peltier, L. Tarasov, G. Vettoretti, L.P. Solheim, Climate dynamics in deep time: modeling the “snowball bifurcation” and assessing the plausibility of its occurrence, in: G.S. Jenkins, M.A.S. McMenamin, C.P. McKay, L. Sohl (Eds.), *The Extreme Proterozoic: Geology, Geochemistry, and Climate*, *Geophys. Mon.*, vol. 146, American Geophysical Union, Washington, DC, 2004, pp. 107–124.
- [22] D. Pollard, J.F. Kasting, Climate-ice sheet simulations of Neoproterozoic glaciation before and after collapse to Snowball Earth, in: G.S. Jenkins, M.A.S. McMenamin, C.P. McKay, L. Sohl (Eds.), *The Extreme Proterozoic: Geology, Geochemistry, and Climate*, *Geophys. Mon.*, vol. 146, American Geophysical Union, Washington, DC, 2004, pp. 91–105.
- [23] K.H. Hoffmann, D.J. Condon, S.A. Bowring, J.L. Crowley, U–Pb zircon date from the Neoproterozoic Ghaub Formation, Namibia: constraints on Marinoan glaciation, *Geology* 32 (2004) 817–820.
- [24] G.P. Halverson, P.F. Hoffman, D.P. Schrag, A.C. Maloof, A.H.N. Rice, Toward a Neoproterozoic composite carbon-isotope record, *Geol. Soc. Amer. Bull.* 117 (2005) 1181–1207.
- [25] B. Goscombe, D. Gray, R. Armstrong, D.A. Foster, J. Vogl, Event geochronology of the Pan-African Kaoko Belt, Namibia, *Precambrian Res.* 140 (2005) 1–41.
- [26] D.R. Grey, D.A. Foster, B. Goscombe, C.W. Passchier, R.A.J. Trouw, $^{40}\text{Ar}/^{39}\text{Ar}$ thermochronology of the Pan-African Damara Orogen, Namibia, with implications for tectonothermal and geodynamic evolution, *Precambrian Res.* 150 (2006) 49–72.
- [27] P.F. Hoffman, 28th DeBeers Alex. Du Toit Memorial Lecture: On Cryogenian (Neoproterozoic) ice-sheet dynamics and the limitations of the glacial sedimentary record, *S. Afr. J. Geol.* 108 (2005) 557–576.
- [28] G.P. Halverson, P.F. Hoffman, D.P. Schrag, A.J. Kaufman, A major perturbation of the carbon cycle before the Ghaub glaciation (Neoproterozoic) in Namibia: prelude to snowball Earth? *Geophys. Geochem. Geosyst.* 3 (2002), doi:10.1029/2001GC000244.
- [29] R.I.F. Trindade, M. Macouin, 2007. Paleolatitude of glacial deposits and paleogeography of Neoproterozoic ice ages, *C. R. Geoscience* 339, 200–211.
- [30] Z.X. Li, S.V. Bogdanova, A.S. Collins, A. Davidson, De Waele, B., R.E. Ernst, I.C.W. Fitzsimons, R.A. Fuck, D.P. Gladkochub, J. Jacobs, K.E. Karlstrom, S. Lu, L.M. Natapov, V. Pease, S.A. Pisarevsky, K. Thrane, V. Vernikovskiy, in press. Assembly, configuration, and break-up history of Rodinia: a synthesis. *Precambrian Res.*
- [31] K.-H. Hoffmann, A.R. Prave, A preliminary note on a revised subdivision and regional correlation of the Otavi Group based on glaciogenic diamictites and associated cap dolostones, *Commun. Geol. Surv. Namib.* 11 (1996) 77–82.
- [32] M.J. Kennedy, B. Runnegar, A.R. Prave, K.-H. Hoffmann, M.A. Arthur, Two or four Neoproterozoic glaciations? *Geology* 26 (1998) 1059–1063.
- [33] A.H. Knoll, M.R. Walter, G.M. Narbonne, N. Christie-Blick, A new period for the geologic time scale, *Science* 305 (2004) 621–622.
- [34] N. Eyles, N. Januszczak, ‘Zipper-rift’: a tectonic model for Neoproterozoic glaciations during the breakup of Rodinia after 750 Ma, *Earth-Sci. Rev.* 65 (2004) 1–73.
- [35] P.F. Hoffman, G.P. Halverson, in press. Otavi Group of the Northern Platform and the Northern Margin Zone. In: Miller, R.McG. (Ed.), *The Geology of Namibia*. Handbook of the Geological Survey of Namibia, Windhoek, Namibia.
- [36] G.P. Eberli, R.N. Ginsburg, Segmentation and coalescence of Cenozoic carbonate platforms, Great Bahama Bank, *Geology* 15 (1987) 75–79.
- [37] E.W. Adams, W. Schlager, Basic types of submarine slope curvature, *J. Sediment. Res.* 70 (2000) 814–828.
- [38] D.J. Condon, A.R. Prave, D.I. Benn, Neoproterozoic glacial–rainout intervals: observations and implications, *Geology* 30 (2002) 35–38.
- [39] E. Domack, P. Hoffman, Stratigraphic transition into and out of a snowball glaciation: evidence from the Otavi Platform and Fransfontein Slope, Namibia, *Eos, Trans. Am. Geophys. Union* 84 (46) (2003) (Fall Mtg Suppl., Abstr. C11B-0819, 2003).
- [40] L.H. King, K. Rokoengen, G.B.J. Fader, T. Gjunleiksrud, Till-tongue stratigraphy, *Geol. Soc. Amer. Bull.* 103 (1991) 637–659.
- [41] S. Xiao, H. Bao, H. Wang, A.J. Kaufman, C. Zhou, G. Li, X. Yuan, H. Ling, The Neoproterozoic Quruqtagh Group in eastern Chinese Tianshan: evidence for a post-Marinoan glaciation, *Precambrian Res.* 130 (2004) 1–26.
- [42] P.A. Allen, P.F. Hoffman, Extreme winds and waves in the aftermath of a Neoproterozoic glaciation, *Nature* 433 (2005) 123–127.
- [43] P. Cloud, L.A. Wright, E.G. Williams, P. Diehl, M.R. Walter, Giant stromatolites and associated vertical tubes from the upper Proterozoic Noonday Dolomite, Death Valley region, eastern California, *Geol. Soc. Amer. Bull.* 85 (1974) 1869–1882.
- [44] F.A. Corsetti, J.P. Grotzinger, Origin and significance of tube structures in Neoproterozoic post-glacial cap carbonates: example from Noonday Dolomite, Death Valley, United States, *Palaios* 20 (2005) 348–363.
- [45] A.C.R. Nogueira, C. Riccomini, A.N. Sial, C.A.V. Moura, T.R. Fairchild, Soft-sediment deformation at the base of the Neoproterozoic Puga cap carbonate (southwestern Amazon craton, Brazil): confirmation of rapid icehouse to greenhouse transition in snowball Earth, *Geology* 31 (2003) 613–616.

- [46] B.W. Logan, P.F. Hoffman, C.D. Gebelein, Algal mats, cryptalgal fabrics and structures, Hamelin Pool, Western Australia, in: B.W. Logan (Ed.), *Evolution and Diagenesis of Quaternary Sequences*, Shark Bay, Western Australia, Mem., vol. 22, American Association of Petroleum Geologists, Tulsa, OK, 1974, pp. 140–194.
- [47] P.U. Clark, J.X. Mitrovica, G.A. Milne, M.E. Tamisiea, Sea-level fingerprinting as a direct test for the source of global meltwater pulse 1A, *Science* 295 (2002) 2438–2441.
- [48] G. Soffer, 1998. Evolution of a Neoproterozoic continental margin subject to tropical glaciation. Unpublished B.A. thesis, Harvard College, Cambridge, Massachusetts, USA, 99 pp.
- [49] W.T. Hyde, T.J. Crowley, S.K. Baum, W.R. Peltier, Neoproterozoic ‘snowball Earth’ simulations with a coupled climate/ice-sheet model, *Nature* 405 (2000) 425–429.
- [50] E. Bard, B. Hamelin, R.G. Fairbanks, A. Zindler, Calibration of the ^{14}C timescale over the past 30,000 years using mass-spectrometric U–Th ages from Barbados corals, *Nature* 345 (1990) 791–794.
- [51] R.I.F. Trindade, E. Font, M.S. D’Agrella-Filho, A.C.R. Nogueira, C. Riccomini, Low-latitude and multiple geomagnetic reversals in the Neoproterozoic Puga cap carbonate, Amazon craton, *Terra Nova* 15 (2003) 441–446.
- [52] B. Kilner, C. Mac Niocaill, M. Brasier, Low-latitude glaciation in the Neoproterozoic of Oman, *Geology* 33 (2005) 413–416.
- [53] T.D. Raub, D.A.D. Evans, Magnetic reversals in basal Ediacaran cap carbonates: a critical review, *Eos, Trans. Am. Geophys. Union* 87 (36) (2006) (Joint Assembly Suppl., Abstr. GP41-02).
- [54] E. Font, R.I.F. Trindade, A. Nédélec, Detrital remanent magnetization in haematite-bearing Neoproterozoic Puga cap dolostone, Amazon craton: a rock magnetic and SEM study, *Geophys. J. Int.* 163 (2005) 491–500.
- [55] P.W. Schmidt, G.E. Williams, The Neoproterozoic climatic paradox: equatorial paleolatitude for Marinoan glaciation near sea level in South Australia, *Earth Planet. Sci. Lett.* 134 (1994) 107–124.
- [56] L.E. Sohl, N. Christie-Blick, D.V. Kent, Paleomagnetic polarity reversals in Marinoan (ca 600 Ma) glacial deposits of Australia: implications for the duration of low-latitude glaciation in Neoproterozoic time, *Geol. Soc. Amer. Bull.* 111 (1999) 1120–1139.
- [57] D. Gubbins, The distinction between geomagnetic excursions and reversals, *Geophys. J. Int.* 137 (1999) F1–F3.
- [58] J.E.T. Channell, B.P. Curtis, B.P. Flower, The Matuyama–Brunhes boundary interval (500–900 ka) in North Atlantic drift sediments, *Geophys. J. Int.* 158 (2004) 489–505.
- [59] C. Laj, C. Kissel, A.P. Roberts, Geomagnetic field behavior during the Iceland Basin and Laschamp geomagnetic excursions: a simple transitional field geometry? *Geochem. Geophys. Geosyst.* 7 (2006) Q03004, doi:10.1029/2005GC001122.
- [60] R.K. Hayward, T.V. Lowell, Variations in loess accumulation rates in the mid-continent, United States, as reflected by magnetic susceptibility, *Geology* 21 (1993) 821–824.
- [61] Z.L. Ding, Z.W. Yu, S.L. Yang, J.M. Sun, S.F. Xiong, T.S. Liu, Coeval changes in grain size and sedimentation rate of aeolian loess, the Chinese Loess Plateau, *Geophys. Res. Lett.* 28 (10) (2001) 2097–2100.
- [62] S.J. Mazzullo, Organogenic dolomitization in peritidal to deep-sea sediments, *J. Sediment. Res.* 70 (2000) 10–23.
- [63] J. Lynch-Stieglitz, T.F. Stocker, W.S. Broecker, R.G. Fairbanks, The influence of air–sea exchange on the isotopic composition of oceanic carbon: observations and modeling, *Glob. Biogeochem. Cycles* 9 (1995) 653–665.
- [64] A.J. Kaufman, A.H. Knoll, G.M. Narbonne, Isotopes, ice ages, and terminal Proterozoic earth history, *Proc. Natl. Acad. Sci. U. S. A.* 94 (1997) 6600–6605.
- [65] G. Jiang, N. Christie-Blick, A.J. Kaufman, D.M. Banerjee, V. Rai, Carbonate platform growth and cyclicity at a terminal Proterozoic passive margin, Infra Krol Formation and Krol Group, Lesser Himalaya, India, *Sedimentology* 50 (2003) 921–952.
- [66] S.A. Kasemann, C.J. Hawkesworth, A.R. Prave, A.E. Fallick, P.N. Pearson, Boron and calcium isotope composition in Neoproterozoic carbonate rocks from Namibia: evidence for extreme environmental change, *Earth Planet. Sci. Lett.* 231 (2005) 73–86.
- [67] A. Neftel, H. Oeschger, J. Schwander, B. Stauffer, Carbon dioxide concentration in bubbles of natural cold ice, *J. Phys. Chem.* 87 (1983) 4116–4120.
- [68] P.A. Allen, J. Leather, M.D. Brasier, The Neoproterozoic Fiq glaciation and its aftermath, Huqf Supergroup of Oman, *Basin Res.* 16 (2004) 507–534.
- [69] F.A. Macdonald, P.F. Hoffman, D.P. Schrag, A thick Ediacaran carbonate succession in Arctic Alaska, *Paleontological Congress, Abstract #T2-16*, Beijing, 2006, pp. 285–286.
- [70] N.M. Lemon, V.A. Gostin, Glaciogenic sediments of the late Proterozoic Elatina Formation and equivalents, Adelaide Geosyncline, South Australia, in: J.B. Jago, P.S. Moore (Eds.), *The Evolution of a Late Precambrian–Early Paleozoic Rift Complex: the Adelaide Geosyncline*, *Geol. Soc. Australia Spec. Publ.*, vol. 16, NSW, Sydney, 1990, pp. 149–163.
- [71] C.R. Calver, M.R. Walter, The late Neoproterozoic Grassy Group of King Island, Tasmania: correlation and paleogeographic significance, *Precambrian Res.* 100 (2000) 299–312.
- [72] M.B. Edwards, Sedimentology of the Upper Proterozoic glacial record, Vestertana Group, Finnmark, Norwegian Geological Survey Bulletin, vol. 394, Geological Survey of Norway, Trondheim, Norway, 1984 76 pp.
- [73] B. Bodiselič, C. Koeberl, S. Master, W.U. Reimold, Estimating duration and intensity of Neoproterozoic snowball glaciations from Ir anomalies, *Science* 308 (2005) 239–242.
- [74] L.J.G. Schermerhorn, W.I. Stanton, Tilloids in the West Congo geosyncline, *J. Geol. Soc. (Lond.)* 119 (1963) 201–241.
- [75] A.J. Kaufman, G. Jiang, N. Christie-Blick, D.M. Banerjee, V. Rai, Stable isotope record of the terminal Neoproterozoic Krol platform in the Lesser Himalayas of northern India, *Precambrian Res.* 147 (2006) 156–185.
- [76] F.A. Corsetti, A.J. Kaufman, The relationship between the Neoproterozoic Noonday Dolomite and the Ibx Formation: new observations and their bearing on ‘snowball Earth’, *Earth-Sci. Rev.* 73 (2005) 63–78.
- [77] M.J. Hambrey, A.M. Spencer, Late Precambrian glaciation of central East Greenland, *Meddelelser om Grønland Geosci.*, vol. 19, Greenland Geological Survey, Copenhagen, Denmark, 1987 50 pp.
- [78] G.P. Halverson, A.C. Maloof, P.F. Hoffman, The Marinoan glaciation (Neoproterozoic) in northeast Svalbard, *Basin Res.* 16 (2004) 297–324.
- [79] G.A. McCay, A.R. Prave, G.I. Alsop, A.E. Fallick, Glacial trinity: Neoproterozoic Earth history within the British–Irish Caledonides, *Geology* 34 (2006) 909–912.
- [80] M. Deynoux, *Essai de Synthèse Stratigraphique du Bassin de Taoudeni*, *Travaux des Laboratoires des Sciences de la Terre*, Saint-Jérôme, Marseille, 1971 71 pp.